IOP Publishing Measurement Science and Technology
Meas. Sci. Technol. **36** (2025) 015002 (12pp) https://doi.org/10.1088/1361-6501/ad801f

Coaxial cable delay measurement with different methods: analyzing influential factors and quantifying numerical effects

Tian Yu[1], **Kun Liang**[1,*], **Zhiyu He**[2], **Hao Liao**[3] and **Jian Wang**[1]

[1] School of Automation and Intelligence, Beijing Jiaotong University, Beijing, People's Republic of China
[2] China Academy of Railway Sciences Corporation Limited, Beijing, People's Republic of China
[3] China Railway Qinghai-Tibet Group Co., Ltd, Xining, People's Republic of China

E-mail: liangk@bjtu.edu.cn

Received 6 June 2024, revised 12 September 2024
Accepted for publication 26 September 2024
Published 14 October 2024

Abstract

Most of the timing scenarios call for the need of precise delay measurement and compensation for coaxial cables. However, experience to date has shown that the cable delay can only be characterized by other physical quantities such as time interval or group delay, etc. In this paper, the principles of three existing commonly used measurement methods were discussed and the various factors that can affect the measurement results were analyzed. Measurement setups and the corresponding uncertainty budgets for the three techniques were then designed and explained. With the aim to quantify numerical effects of the influential factors, specific experiments on a 50 m antenna cable were conducted on time interval measurement to obtain the optimal range of the instrument's trigger level based on external pulses with different rise time settings, as well as on group delay measurement to determine the influence of different frequency aperture settings. Then, experiments using the relatively proper parameters, which we believe, to the optimal extent, would mitigate the measurement uncertainties were performed. In order to ensure the measurement consistency across the methods, the measurement results were compared and cross-validated to obtain the recommended selections of parameters to align the measurements for coaxial cable delay utilizing the different methods.

Keywords: time transfer, cable delay, GNSS, calibration, measurement

1. Introduction

In timing systems such as network time service systems, and global navigation satellite system (GNSS), the majority of devices are connected through coaxial cables in order to transmit signals. Typical examples include the coaxial cables utilized for the transmission of 1 Pulse Per Second (1PPS) signals between the reference clock and the GNSS receiver input. Also, in the context of GNSS calibration, the cable delay has been described as the frequency-independent signal group delay inside the antenna cable [1]. Uncalibrated cables can introduce systematic errors ranging from several tens to hundreds of nanoseconds, which is insufficient for nanosecond-level time transfer and other GNSS timing scenarios. Additionally, even with the introduction of cable delay calibrations, the measurement uncertainty should also be optimized to ensure the overall uncertainty in such applications to remain as low. Thus, measurements for the time delay of such cables to compensate is an essential work.

* Author to whom any correspondence should be addressed.

Experience to date, however, has shown that several different kinds of measurements are used for quantifying the cable delay and the transmission delay of any signal through a cable depends on several factors.

Currently, the measurement of the cable delay is mainly carried out by the time interval counter (TIC)-based time interval measurement, which is regarded as the most flexible and accessible option available today. Its disadvantage is that the instrument response will be strongly influenced by the pulse shape of the signals through the cable under test [2, 3]. Besides, in 2003, an inter-laboratory comparison called TF.TI-K1 was conducted by the European Association of National Metrology Institute [4], with the participation of 25 National Metrology Institutes in total, which were free to choose their own method to measure the time delay of 3 cables with different lengths in a black box in turn. The results revealed measurement inconsistencies of approximately 1 ns on a 4 m cable, 0.5 ns on a 10 m cable, and nearly 2 ns on a 35 m cable. Although 24 out of the 25 participants applied TICs for measurements, the discrepancies still indicated an underperforming level of measurement uncertainty under such circumstances that the procedures and the instrument settings were not strictly demanded to be aligned. Other cable delay measurement techniques represented by vector network analyzer (VNA)-based group delay measurement and pseudorange difference measurement using a GNSS simulator have also been adopted for antenna cable delay measurements in time link calibrations according to [5, 6], which are evaluated with a lower level of uncertainty, but have slight difference in the parameter settings of the instrument. These methods have preliminarily been reviewed and discussed in [7].

Techniques of 1PPS reflection, $\lambda/2$ resonator reflection and VNA reflection are also introduced for *in-situ* antenna cables in [8]. As the recommendation in the Annex 1 of the BIPM Guidelines for GNSS Calibration is to complete the calibration of all components prior to the installation of the system [9], and moreover, due to the frequent utilization by the majority of laboratories, the study in this paper will be limited to cable measurements using transmission methods.

By now, the lack of standardization in measurement method of coaxial cable delay is evident. Even when utilizing the same instrument, discrepancies in the parameter settings can still impact the results. In this paper, the three commonly used measurement methods for coaxial cable delay were analysed and discussed theoretically and experimentally to identify and quantify the potential influential factors on them, which were later validated in sequence. The experimental setups for measurements and corresponding uncertainty evaluations were designed to extract the certain adjustable parameters that need to be considered to improve the measurement uncertainty. Further investigations were conducted to obtain the proper parameter selection ranges through several traversal experiments. Results were compared to finally ensure the alignments across the three available measurement methods.

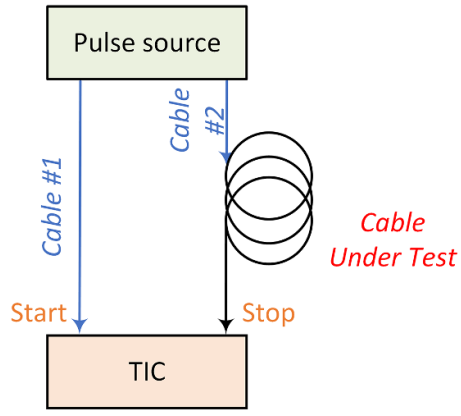

Figure 1. Schematic of the time interval measurement.

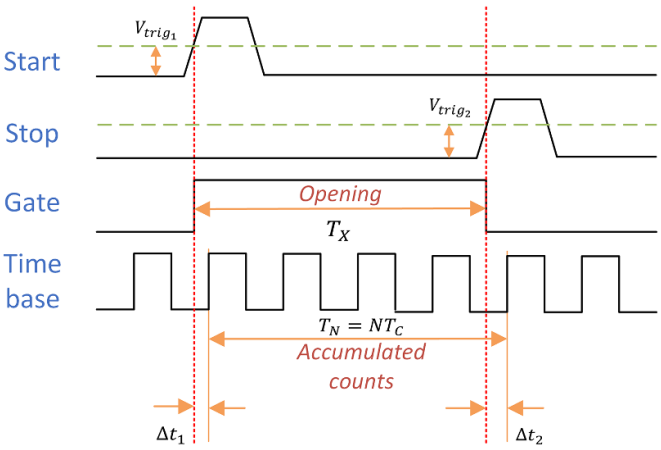

Figure 2. Simplified illustration of time interval measurement.

2. Analysis for influential factors on different measurement methods

In this section, the corresponding experimental setups and principles underlying the three methods were respectively depicted to analyse the potential influential factors during the measurements.

2.1. Time interval measurement

Time interval measurements utilizing the TICs are usually performed with the assistance of an external pulse source as shown in figure 1, which can be the 1PPS signals distributed by a regenerative pulse distribution amplifier (PDA).

The result is derived by subtracting the time interval measured before and after the cable under test is inserted. Both cables #1 and #2 are arbitrary cables but must be held in place during the measurement.

The time interval, defined as the duration between specific start and stop events, is typically measured by the time elapsed between the first and second triggering edges of the TIC as shown in figure 2.

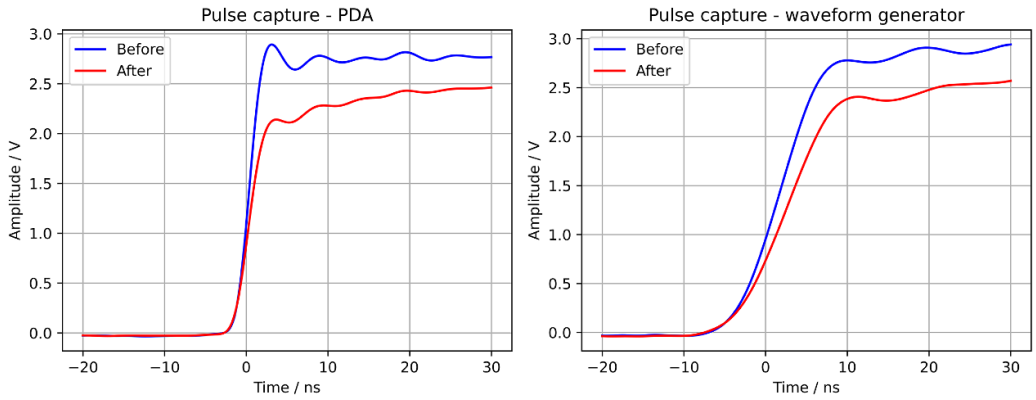

Figure 3. Pulses observed before (blue) and after (red) passing through a 50 m antenna cable.

The gate is opened when the start event is triggered at a certain level V_{trig_1}, and is closed V_{trig_2}, while the accumulated counts of the time base pulse will be included in the calculation with the error terms Δt_1 and Δt_2 [10]. The time difference between the Start and Stop events can thus be obtained from equation (1),

$$T_X = NT_C + \Delta t_1 - \Delta t_2 = T_C\left(N + \frac{\Delta t_1 - \Delta t_2}{T_C}\right) \tag{1}$$

T_X: time interval measurement;
N: number of clock pulses of the time base;
T_C: a cycle of the time base pulse;
Δt_1: time difference between the start event and the first counting pulse edge after the count starts;
Δt_2: time difference between the stop event and the first counting pulse edge after the count ends.

The measurement error derived from this method can be expressed as equation (2),

$$\delta = \Delta t_1 - \Delta t_2 \ . \tag{2}$$

While a counter with a time base of frequency f offers a resolution of $\frac{1}{f}$, further enhancing time resolution necessitates interpolation techniques like the Nutt method, as discussed in [11].

Due to the nature of pulse signals, promote investigation is required to determine the optimal measuring settings of the instrument, as opposed to sinusoidal signals where [12] has established guidelines for selecting the optimum trigger level. Pulse signals often exhibit wide spectral content with high-frequency components, making them susceptible to distortion when transmitted through coaxial cables, which typically experience significant attenuation at higher frequencies. Consequently, both the pulse characteristics of the measured time signal and the physical properties of the cable will influence the measurement outcomes. The distorted pulses through an antenna cable obtained using PPS sources with different features are presented in figure 3. The pulses are input from the 1PPS output of a disciplined rubidium clock distributed by an external PDA and an arbitrary waveform generator, respectively. The PDA is capable of providing pulses with amplitudes of 3.0 V and rise times of approximately 3 ns when terminated to a 50 Ω load. The output of the generator was also set to produce pulses with an amplitude of 3.0 V, but rise times of 10 ns under the same condition. Note that both images were taken with an oscilloscope at a trigger level of 1.0 V and the two pulses inside were manually realigned referenced to the first sample point off the 0 V horizontal line for experimental presentation.

A reduction in pulse amplitude and an increase in rise time can be clearly seen. Attenuation is particularly noticeable at the end of the rising edges of the pulses, consequently leading to overestimations of the time interval measurements when the trigger levels are set to higher volts.

We have also used four short coaxial cables of 1 m in length, modelled PHC260, PH18, PH18S and PH223 respectively, to capture the pulse distortion input from the external PDA. The short cables differ in structural characteristics as detailed in table 1, and consequently in their electrical characteristics. The pulses from the same source likewise have different distortion characteristics passing through, as shown in figure 4. Note that all images were taken using the same way as in figure 3.

2.2. *Group delay measurement*

The measurements conducted by VNAs are usually derived by the S21 parameters in group delay with both ports of the instrument calibrated to the Radio Frequency (RF) connector of the cable under test, as shown in figure 5.

Group delay is a parameter that has been widely used in the field of RF to describe the linear distortion of a given transmission network. It is mathematically defined as the negative derivative of phase in radian with respect to frequency, as shown in equation (3). For a 2-port RF network under test without frequency conversion, e.g. a coaxial cable, the group delay will also be a measure and characterization of the absolute signal delay [13],

$$\tau(f) = -\frac{1}{2\pi}\frac{d\varphi(f)}{df} \ . \tag{3}$$

Table 1. Structural characteristics and according materials or typical values of the four 1 m short coaxial cables under test.

Structural characteristics		Materials/Typical values			
		PHC260	PH18	PH18S	PH223
Inner Conductor	Material	Silver plated copper	Silver plated copper	Silver plated copper	Silver plated copper
	Nom. Dia (mm)	0.53	1.44	1.45	0.90
Insulation	Material	Solid-PTFE	LD-PTFE	LD-PTFE	PE
	Nom. Dia (mm)	1.68	3.99	3.85	2.95
Inner shield	Material	Silver plated copper strip	Silver plated copper strip	Silver plated copper strip	Silver plated copper strip
	Nom. Dia (mm)	1.88	4.19	4.05	3.50
Outer shield	Material	Silver plated copper wire	Silver plated copper wire	Silver plated copper wire	Silver plated copper wire
	Nom. Dia (mm)	2.20	4.90	4.85	3.95
Sheath	Material	FEP	FEP	FEP	PVC
	Nom. Dia (mm)	2.60	5.40	5.40	5.30

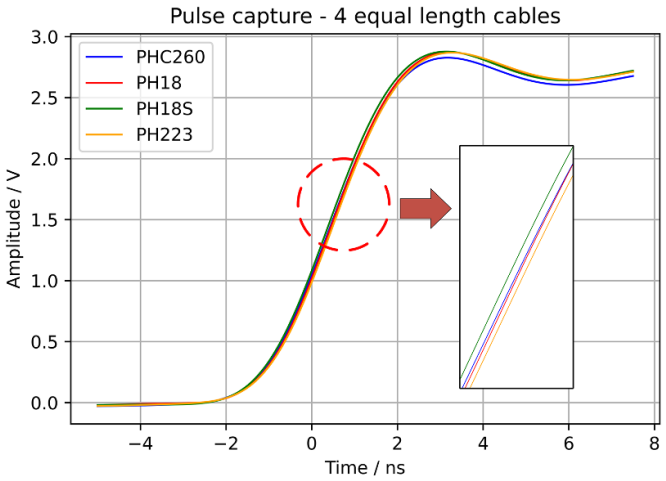

Figure 4. Pulses observed after passing through 1 m cables.

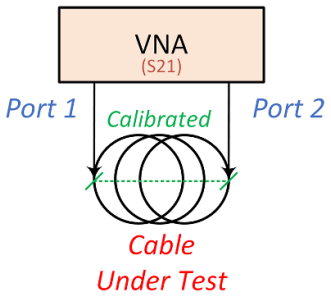

Figure 5. Schematic of the group delay measurement.

The scatter parameters (S-parameters) serve as the reference parameters for describing the magnitude and phase characteristics of RF networks and are commonly employed in VNAs. Among the S-parameters, S21 is usually utilized for measuring the insertion loss and phase variation of a network under test. This parameter quantifies the changes in amplitude and phase at a specific frequency, relative to its known amplitude and phase, as it propagates through the network and emerges at the output port. During an S21 measurement, the VNA initially determines the phase response at the frequency f to obtain the group delay according to equation (4),

$$\tau_g(f) = -\frac{1}{2\pi}\frac{\varphi\left(f+\frac{\Delta f}{2}\right)-\varphi\left(f-\frac{\Delta f}{2}\right)}{\Delta f} \tag{4}$$

$\tau_g(f)$: group delay obtained at frequency f;
$\varphi(f)$: phase response measured at frequency f;
Δf: sampling interval of phase response in the frequency domain, i.e. the frequency aperture.

It is crucial to consider that S21 can only measure phase responses within the range of $(-\pi, \pi)$ for a given frequency stimulus. Thus, phase expansion becomes essential to resolve the 2π ambiguity, necessitating a 2π subtraction when the phase difference between consecutive measurements exceeds 2π. Moreover, the maximum frequency aperture setting should not exceed the range where the phase response of the network under test surpasses 2π. This precaution is vital to prevent erroneous group delay measurements stemming from overlooking the fine details in phase.

To illustrate, figure 6 provides a simulated diagram of the aforementioned. Under normal circumstances as shown by the red dots, the group delay measurement will be obtained using the raw phase samples from both ends of a frequency aperture as equation (4). For measurement involving 2π phase jumps, as indicated by the blue dots, the adjacent phase measurement will subtract 2π prior to engaging in arithmetic. At excessive aperture settings, represented by the green dots, the phase-frequency curve will incorrectly resemble the yellow dashed line in the figure. Therefore, the selection of the frequency aperture needs to satisfy the following equation, requiring potential delay estimation before measurement,

$$\Delta f < -\frac{1}{2\pi}\frac{\max\left(\varphi\left(f+\frac{\Delta f}{2}\right)-\varphi\left(f-\frac{\Delta f}{2}\right)\right)}{\tau_g(f)} = \frac{1}{\tau_g(f)} \tag{5}$$

According to [14], the time delay of a coaxial cable is related to its mechanical length through the permittivity of the dielectric material within the cable, expressed in equation (6),

$$\tau = \frac{L_{\text{mech}} * \sqrt{\varepsilon}}{c} \tag{6}$$

τ: delay time of the cable under test;
L_{mech}: mechanical length of the cable under test;
ε: permittivity of the dielectric material within the cable;

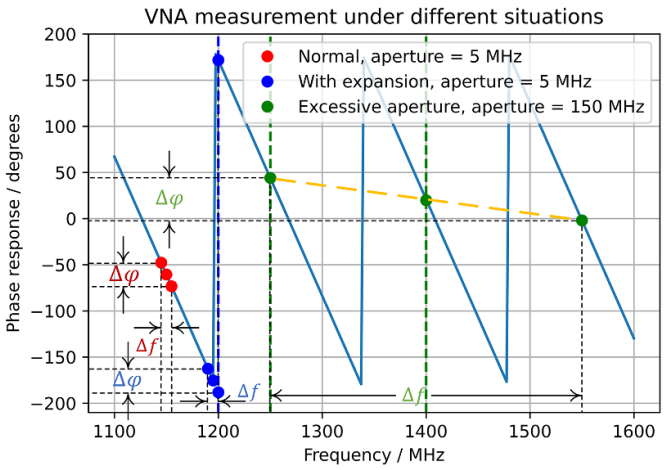

Figure 6. Phase response under 3 different situations of a simulated device under test using a VNA.

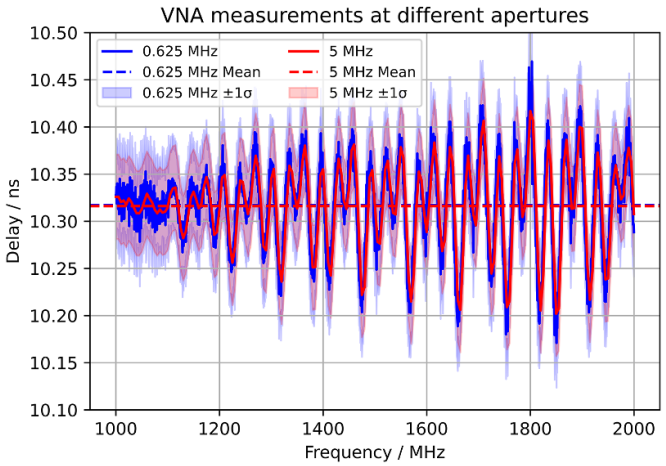

Figure 7. VNA measurements of a 2.5 m coaxial cable at respectively the maximum and the minimum aperture settings. Dashed lines indicate the mean values of the measurements, and shaded areas indicate the 1-σ error ranges of the measurements.

c: velocity of light.

For instance, the permittivity of the RG-58 coaxial cable type is typically between 2.3 and 2.4. Thus, the delay of a 50 m cable can be estimated at approximately 253 ns. Therefore, according to equation (6), the maximum frequency aperture should not exceed 4 MHz approximately.

Furthermore, to assess the potential discrepancies resulting from different aperture settings within the specified constraints, the results depicted in figure 7 compare measurements of a 2.5 m cable obtained at both the maximum 5 MHz and minimum 0.625 MHz aperture settings achievable under (1-2) GHz stimulus by a commercial VNA. It is noticeable that if a wider aperture is chosen, the resolution of group delay measurements relative to frequency will be lower, thus causing more detailed observation to be undetected. However, less jitter will be introduced due to the indirect filtering compared to a narrower aperture.

As the previous TIC measurement, the VNA measurement is also dependent on the transmission characteristics of the

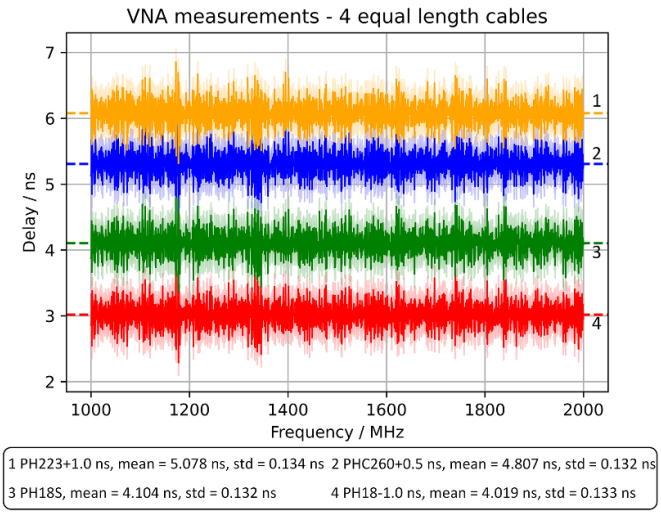

Figure 8. Group delay measurements of the four equal length coaxial cables using a VNA. Plots of the PH223, PHC260 and PH18 have been shifted +1.0 ns, +0.5 ns and −1.0 ns, respectively, for better viewing.

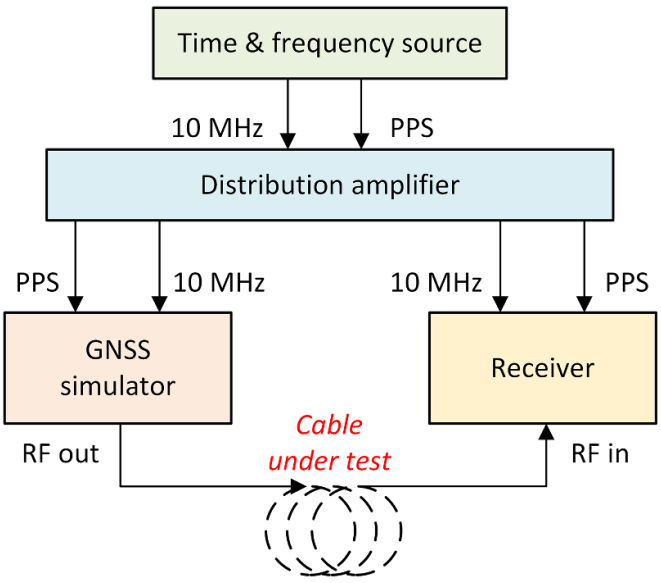

Figure 9. Scheme of the pseudorange simulation measurement.

cable under test. The results of the VNA measurements for the four equal length coaxial cables over (1-2) GHz are presented in figure 8.

2.3. *Pseudorange simulation measurement*

The schematic of pseudorange simulation measurement is shown in figure 9.

In the scope of GNSS, pseudorange refers to the apparent range or distance between a GNSS receiver and a satellite, as measured by the receiver. A GNSS constellation simulator is an instrument capable of generating artificial GNSS signals, which can be synchronized to the identical external time and frequency reference fed to the receiver host, with preset

pseudorange while disabling environmental factors that influence (e.g. ionosphere, troposphere and multipath, etc). Ideally, therefore, by establishing the experimental setup where both the GNSS simulator and the receiver are connected to the same clock reference, the pseudorange observed by the receiver should be identical to that generated by the simulator, but will inherently exhibit differences due to the various hardware delays among the RF transmission path after compensating for the reference delay, as expressed in equations (7) and (8).

$$\Delta \mathrm{pr}_0 = \tau_{\mathrm{int}} - \tau_{\mathrm{ref}_0} + t_{\mathrm{RFcable}} + t_{\mathrm{SD}} \tag{7}$$

$$\Delta \mathrm{pr}_1 = \tau_{\mathrm{int}} - \tau_{\mathrm{ref}_1} + (t_{\mathrm{RFcable}} + t_{\mathrm{CUT}}) + t_{\mathrm{SD}} \tag{8}$$

$\Delta \mathrm{pr}_i$: the pseudorange difference obtained between the receiver and the simulator with or without cable insertion;

τ_{int}: hardware delay of the receiver;

τ_{ref_i}: delay between the receiver clock and the external reference;

t_{RFcable}: delay of the cables used on the RF transmission path;

t_{CUT}: delay of the cable under test;

t_{SD} : hardware delay of the simulator.

Thus, it is feasible to obtain the cable delay by measuring the $\Delta \mathrm{pr}_1$ when inserting a cable under test into the RF path of the experiment setup, and deducting $\Delta \mathrm{pr}_0$ observed without the cable insertion then. The receiver is capable of generating continuous receiver independent exchange format files to log the observed pseudorange data in both scenarios with and without the cable insertion. The $\Delta \mathrm{pr}_i$ will then calculated by a method similar to the common view, i.e. based on the receiver observing the same satellites as those broadcasted by the simulator at the same moments, and deducting the corresponding code observations from the simulator's preset.

Note that in the experiments with and without cable insertion, we have considered the internal hardware delays of the receiver and the simulator as constants, but it is possible that the τ_{ref} may vary depending on the external clock synchronization between the simulator and the receiver, additional measurements are therefore required. As the signals passing through the cable under test in this method are the closest to those in real GNSS environment, the method is often regarded as more appropriate for antenna cable measurements. Owing to its relatively fixed experimental layout, its influential factors can be considered negligible, and thus can be regarded as the reference measurement for further validations.

3. Uncertainty budget

This section will present the corresponding uncertainty budge for the methods that have been previously described, which will enable the derivation of the influential factors that directly contribute to the overall measurement uncertainty.

According to the specification of SR620 [15], the time interval error derives from resolution, time base error, trigger level error and the system error. Thus, the uncertainty of time interval measurement can be derived by equation (9),

$$u_{\mathrm{cab}} = \sqrt{({u_{\mathrm{res}}}^2 + {u_{\mathrm{clk}}}^2 + {u_{\mathrm{trig}}}^2 + {u_{\mathrm{sys}}}^2 + {u_{\mathrm{rep}}}^2)}. \tag{9}$$

The component introduced by the resolution of TIC is given by u_{res} with a value of 25 ps, the time base error given by u_{clk}, which can be neglected using an highly accurate external frequency source, the trigger error by u_{trig} according to equation (10), the system error by u_{sys} with a ceiling of 500 ps and the repeatability by u_{rep}, taken from the jitter of measurements under multiple runs,

$$u_{\mathrm{trig}} = \frac{15\,mV + 0.5\% V_{\mathrm{trig}}}{k_{\mathrm{PPS}}} \tag{10}$$

V_{trig}: trigger level of the measurement channel;

k_{PPS}: slew rate of the measured PPS.

Previous studies have shown that the uncertainty of the TIC method is always evaluated to be higher than 500 ps when applied to a cable with high attenuation [8], while that of the VNA method to be lower than 100 ps when applied to a well performing cable and the simulator method 200 ps. However, the procedures for detailed uncertainty evaluation are not so clearly explained in the source text. Additionally, we believe that the latter two may be too small, as will be explained later.

The uncertainty budget for group delay measurement can be expressed by equation (11),

$$u_{\mathrm{cab}} = \sqrt{({u_{\mathrm{cal}}}^2 + {u_{\mathrm{def}}}^2 + {u_{\mathrm{tem}}}^2 + {u_{\mathrm{con}}}^2 + {u_{\mathrm{rep}}}^2)}\ . \tag{11}$$

The component introduced by the initial calibration of the two ports of the VNA is given by u_{cal} with a value of about 200 ps extracted from the according datasheet, the cable deformation by u_{def} with 150 ps according to [16], the temperature effect by u_{tem} with 50 ps, which is a conservative value estimated by the sensitivity factor of 0.01 available at: for an RG-58 cable with the time length of 41 ns, given in [17], the connectors by u_{con} with 150 ps, estimated using 75 ps each, which is evaluated using an average from the measurements of several connectors connected in series with VNA, and the repeatability by u_{rep}, taken from the jitter of the measurements.

The uncertainty of the method using a GNSS simulator is given in equation (12),

$$u_{\mathrm{cab}} = \sqrt{({u_{\mathrm{ICBs}}}^2 + {u_{\mathrm{tem}}}^2 + {u_{\mathrm{swi}}}^2 + {u_{\mathrm{RFin}}}^2 + {u_{\mathrm{rep}}}^2)}\ . \tag{12}$$

The component introduced by the inter channel bias of the simulator is given by u_{ICBs} with a value of 10 ps, which is the maximum measured bias with the receiver, the temperature effect by u_{tem} with 192 ps, which is a conservative value calculated taking the factor of 0.083 available at: for fellow time and frequency transfer receivers given in [17], the switching characteristics by u_{swi} with 75 ps, which is the maximum bias of the time difference converted from the pseudorange data collected by the receiver with restart, the RF input level by u_{RFin} with 100 ps according to [6], and the repeatability by u_{rep}, taken from the jitter of the measurements.

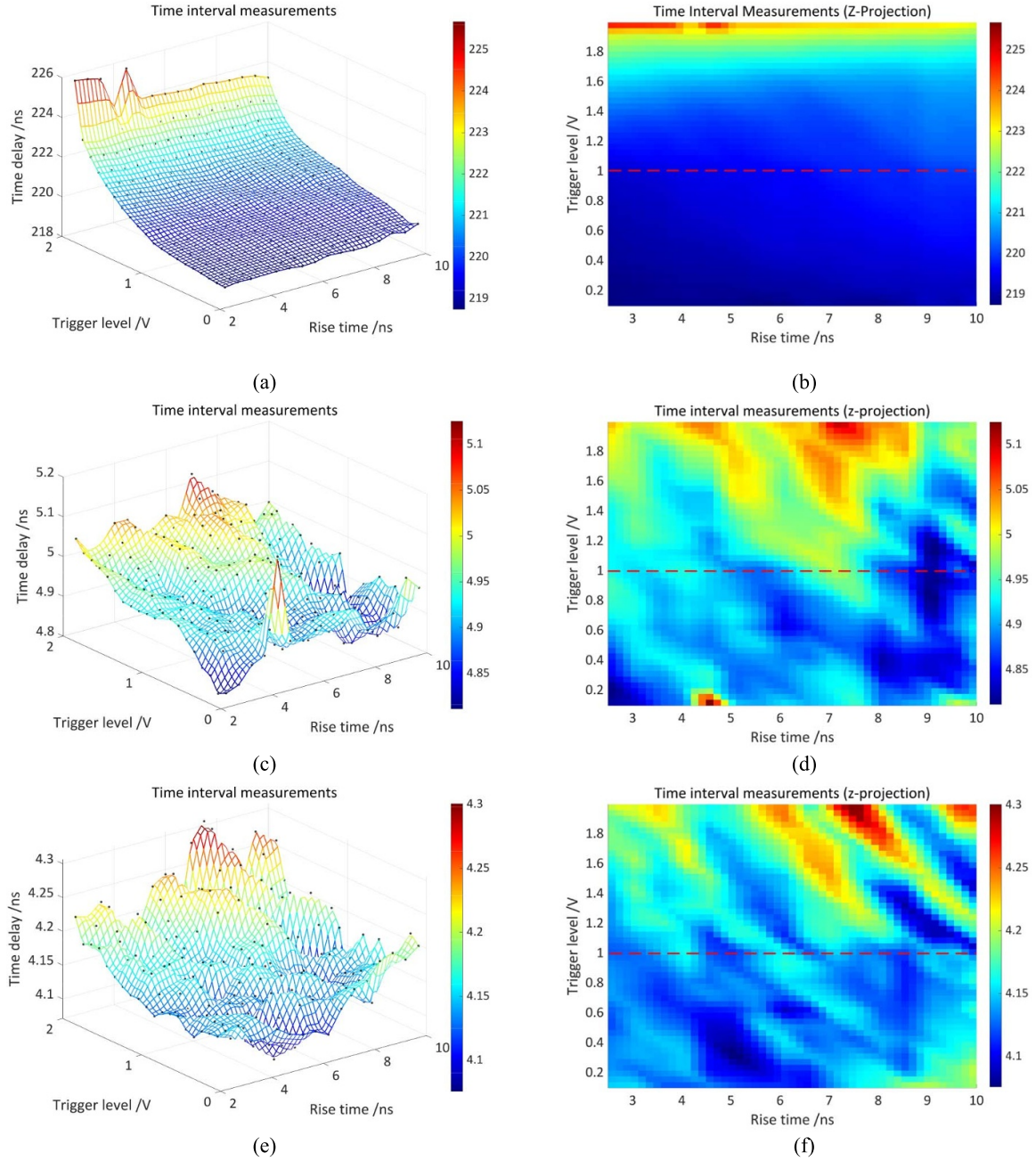

Figure 10. (a) Measurements of time interval during parameter traversal for 5D-FB cable. The black dots represent the raw measurements and the grid plot is derived by interpolation using triangulation to obtain a smoother distribution of the data, the same below. (b) The z-projections of the traversed results after interpolation for 5D-FB cable. The red dashed line represents the measurements derived from 1.0 V triggers. (c) Measurements of time interval during parameter traversal for PHC260 cable. (d) The z-projections of the traversed results after interpolation for PHC260 cable. (e) Measurements of time interval during parameter traversal for PH18 cable. (f) The z-projections of the traversed results after interpolation for PH18 cable. (g) Measurements of time interval during parameter traversal for PH18S cable. (h) The z-projections of the traversed results after interpolation for PH18S cable. (i) Measurements of time interval during parameter traversal for PH223 cable. (j) The z-projections of the traversed results after interpolation for PH223 cable.

The overall uncertainty of the VNA method and the method using a GNSS simulator applied for the preliminary experiment can be finally reduced to approximately 360 ps and lower than 300 ps, respectively.

It can be revealed that, with the aim of improving measurement uncertainty, proper strategies for the mitigation of certain contributions need to be considered, which call for the optimized selections for adjustable influential parameters, that is, the external pulse rise time and the TIC trigger level to minimize u_{trig} in time interval measurement and the frequency aperture to balance u_{rep} and measurement resolution in group delay measurement, as will be discussed in section 4.

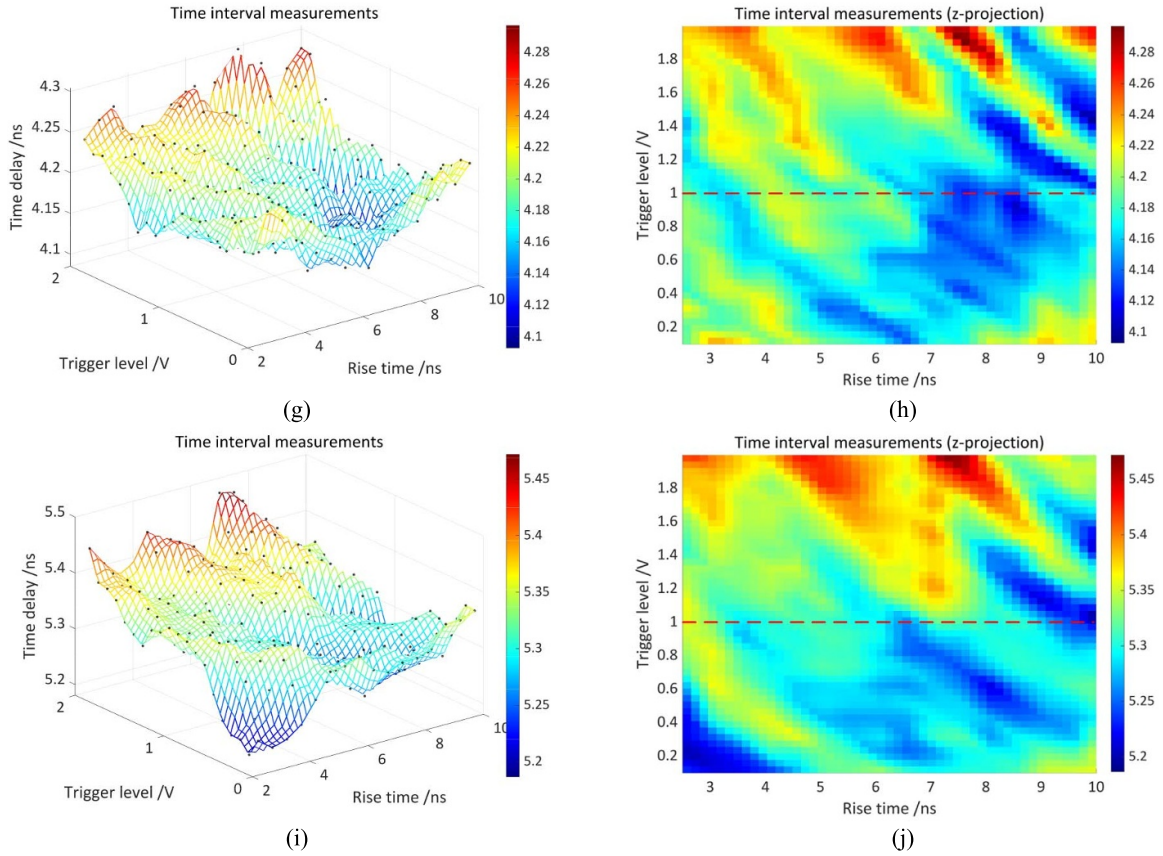

Figure 10. (Continued.)

4. Numeric effects of influential parameters on delay measurements

In this section, a series of experiments were carried out to quantify the influences of the discussed factors, that is, the external pulse rise time and the counter's trigger level for TIC method and the frequency aperture for VNA method, to derive the optimal selections of the parameters, respectively.

4.1. Time interval measurement: determining proper external pulse rise time and the TIC trigger level

The experiments of TIC method were performed on a 50 m coaxial cable modelled 5D-FB and the four 1 m coaxial cables listed in table 1, where we utilized an arbitrary waveform generator modelled RIGOL DG5352 instead of the PDA to make the time pulse characteristics controllable and the counter we used was a standford research system SR620.

The amplitude of the pulse was set to 3.0 V terminated to 50 Ω, and the pulse width to 10 μs to align with the mentioned regenerative PDA. The rise time was increased from 2.5 ns to 10 ns with a step of 0.5 ns to emulate different external pulses, and at each setting of the rise time, the trigger level of the TIC would be traversed from 0.1 V to 2.0 V with a step of 0.1 V. The results are given in figure 10. In order to establish a reference measurement, the results obtained through the use of the BIPM-recommended 1.0 V triggers are highlighted.

For the 50 m 5D-FB cable, by looking at the *x*-axis which represents the TIC trigger level, it can be observed that the pulse rise time is prolonged due to the pulse distortion as described in section 2.1, resulting in a Stop signal delay at high trigger levels to cause the overestimation. It is also worth noting that, as in figure 10, when looking at the *y*-axis, which represents the rise time setting of the pulse source, at trigger levels below 1.6 V the time delay will increase as the pulse rise time increases while at above performs the opposite. This can be seen as evidence that faster pulses have more attenuation through the cable at the end of the rising edge due to the higher frequency component.

For the 1 m cables, the similar delay overestimation with the rise of pulse rise time and the trigger level that has been observed during the 50 m coaxial cable experiment is alleviated due to the negligible distortion of pulse passing through the cables. Additionally, the measurement fluctuations are more reflective of the inherent measurement uncertainty.

In general, the measurement offset for long cable introduced by trigger level can reach a maximum of nearly 8 ns. Thus, for measurements of cables with high attenuation, the parameter range should be maintained as far to the bottom left of the image as possible, i.e. to increase the PPS slope by minimizing external pulse rise time while simultaneously reducing

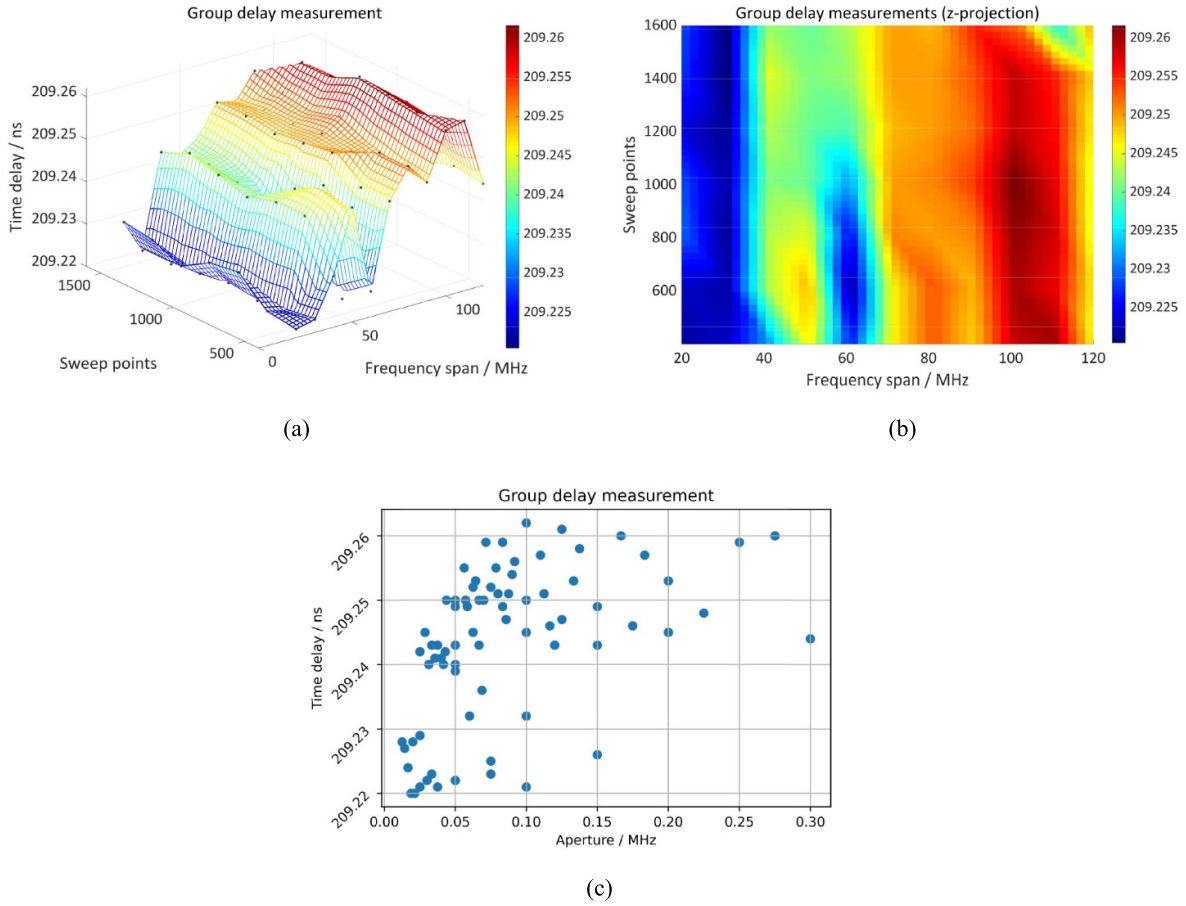

Figure 11. (a) Measurements of group delay during parameter traversal. The black dots represent the average mean values of 10 measurements taken under specific parameters, and the grid plot is derived by interpolation using the same method as in figure 10 to obtain a smoother distribution of the data. (b) The z-projections of the traversed results after interpolation. (c) Converted aperture-mean scatter plot of the measurements during parameter traversal.

counter trigger level to ultimately reduce the contribution of u_{trig} for both channels.

4.2. Group delay measurement: quantifying the influence of frequency aperture

The group delay measurements were performed on another 50 m cable, using a VNA modelled Transcom T5260C, with both ports calibrated to the cable connectors prior to implementation. As stated in section 2.2, the VNA's group delay measurement relies on phase measurement, which requires consideration of the potential 2π ambiguity. According to equations (5) and (6), the maximum frequency aperture for an RG-58 like 50 m coaxial antenna cable is about 4 MHz.

Here we started with the centre frequency of GPS L1, to perform another parameter traversal experiment with a span from approximately equal to the signal bandwidth, 20 – 120 MHz, where the sweep points would traverse from 401 to 1601 to indirectly traverse the frequency aperture from 0.0125 MHz to 0.3 MHz, well below the upper limit of 4 MHz that could result in incorrect measurements as discussed earlier. The measurements within the GPS L1 bandwidth were taken to be averaged to obtain the final result. For each set of specific parameters, the VNA would perform 10 runs to record the mean and standard deviation values. The measurement results are presented in figures 11 and 12.

Figure 11 shows that the maximum difference between the measurement results under various settings is lower than 50 ps, indicating good consistency in the VNA measurement. Furthermore, as mentioned in section 2.2, a narrower aperture setting will yield more measurement details but will also increase the measurement jitter. This has been demonstrated and quantified in figure 12. When the frequency span is set to below 50 MHz, increasement in the standard deviation will become more apparent as the setting of sweep points raises, numerically reaching above 0.3 ns. Although a smaller frequency aperture is often recommended to achieve higher resolution, it is quantitatively advisable not to go lower than 0.05 MHz to avoid an increase in u_{rep}.

5. Ensuring alignment among different measurement methods

Based on the parameters that were derived relative to the preceding analysis of specific experimental setup, we conducted measurements on a 50 m antenna cable along with 4 ordinary

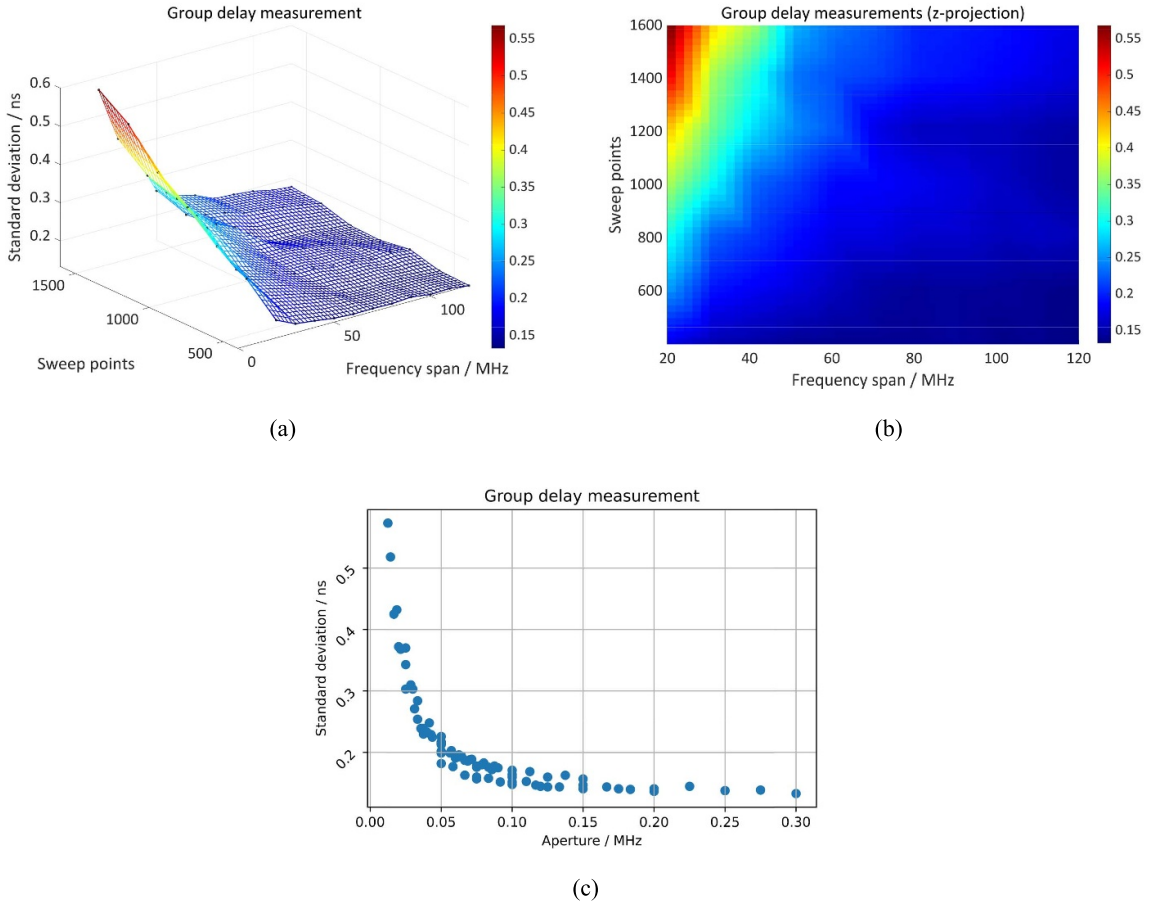

Figure 12. (a) Standard deviation of the measurements during parameter traversal. The black dots represent the maximum standard deviation of 10 measurements taken under specific parameters, and the grid plot is derived by interpolation using the same method as in figure 10 to obtain a smoother distribution of the data. (b) The z-projections of the traversed results after interpolation. (c) Converted aperture-standard deviation scatter plot of the measurements during parameter traversal.

Table 2. VNA parameters for the measurement.

Parameters	Value
S-parameter	S21
Format	Group delay
Average factor	16
Smoothing	off
Frequency span	1 GHz to 2 GHz
IF bandwidth	1 kHz
Sweep points	1601
Power level	−20 dBm

coaxial cables of 1 m long using the three aforementioned setups.

Due to the PDA in use produces pulses with rise times of about 3.0 ns, a moderate 1.0 V was selected for TIC measurements, and the results were obtained by averaging 20 adjacent samples. The detailed parameter configuration for the VNA method is shown in table 2. The IF bandwidth was set to 1 kHz to balance the dynamic range with a moderate sweep time. A span of (1–2) GHz was chosen to cover all the available GNSS carriers, with the sweep point set at the maximum of 1601 to give an aperture of 0.625 MHz, as a compromise between resolution and measurement jitter. To avoid the effects of background noise, the stimulus power level was set at −20 dBm. The final result of the measurement was obtained by the group delay data averaged over two frequency bands around (1.16–1.31) GHz and (1.52–1.62) GHz respectively in one scan. For the reference pseudorange simulation measurement, we used a Spirent GSS8000 simulator to provide GNSS-like signals in GPS L1C/A. The receiver we used was a homemade GNSS time transfer receiver (type TLab-TFS-G1). The results were obtained by averaging over the sampling period in one experiment.

Table 3. Measurement results (ns).

Instrument	Carriers/Codes	Measured delay				
		5D-FB	PH223	PHC260	PH18S	PH18
TIC	/	219.21	5.12	4.85	4.13	4.04
VNA	1.16–1.31 GHz	218.63	5.08	4.81	4.10	4.02
	1.52–1.62 GHz	218.62	5.08	4.81	4.10	4.02
GNSS simulator	GPS L1C/A	218.64	5.16	4.96	4.24	4.00

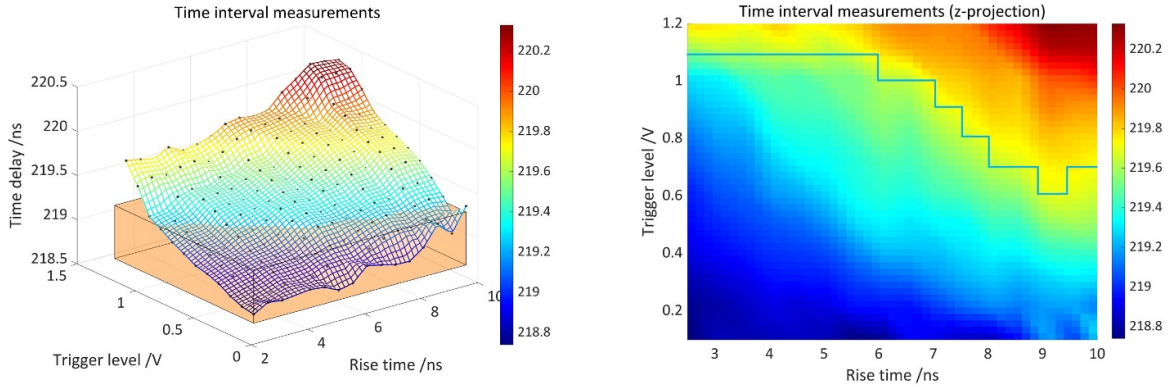

(a) (b)

Figure 13. (a) Scaled plot of the measurements of time interval. (b) The z-projections of the scaled data.

Table 4. Recommended trigger level configuration at corresponding rise times.

Rise time (ns)	Recommended trigger level (V)
(2.5-5.5)	<1.1
6.0, 6.5	<1.0
7.0	<0.9
7.5	<0.8
8.0, 8.5	<0.7
9.0, 9.5	<0.6
10.0	<0.7

All results are presented in table 3, which were largely consistent, with several hundred picoseconds falling within the uncertainty range. The TIC measurement, although in agreement within the uncertainty range, still showed an overestimation of the measured time delay, which we assume probably still due to the trigger level timing error caused by the pulse distortion.

Given the pervasive utilization of the TIC method, to demonstrate this numerical relationship, and to ensure measurement alignments across the methods, figures 10(a) and (b) have been scaled to figures 13(a) and (b) by limiting the x-axis coordinates, that is, the trigger level to be less than 1.2 V. The orange translucent cubes in figure 13 (a) illustrate the results with 1-σ uncertainty of the reference pseudorange simulation measurements, respectively. Figure 13 (b) is divided into two parts by the light blue line. The lower part displays measurements that align with the results obtained the GNSS simulator within the uncertainty range. Quantitatively, it is advisable to configure the trigger level based on different rise times highlighted in table 4.

6. Conclusion

Generally, up until now, the methods available for the measurement are all achieved by indirectly characterizing cable delay through other physical quantities such as time interval, group delay or pseudorange difference, etc. This results in an initial discrepancy in the actual measured objects, and further ones in the applied instruments with detailed procedures.

In this paper, the principles and potential influential factors of the three most commonly used transmission measurement methods for coaxial cable delay at present were mainly discussed and analysed. The detailed measurement setups with corresponding uncertainty budget were designed. In the case of time interval measurement, we assume that the main error may derive from the inappropriate setting of trigger level in the presence of pulse distortion caused by attenuation of high frequency components. The device is the most accessible to use due to its flexibility and wide range of applications. However, it is accompanied by ahigh degree of measurement uncertainty for cables exhibiting high attenuation. For

group delay measurement, the effects of aperture settings were investigated. This method is comparable to the time interval measurement in convenience, with correspondingly more optimal measurement uncertainty, but the standard reference parameter settings remain inconclusive. And the pseudorange simulation measurement was considered as the one closet to real GNSS applications with a relatively fixed experimental setup. One disadvantage of this approach is the high cost and the difficulty of simulating complete GNSS constellations.

To quantify the impacts of the discussed influential factors, and to derive the proper selection of the instruments' parameters, the discrepancy was attempted to be characterized in combination with the influential factors that will directly influence the overall uncertainty of the time interval measurement through a parameter traversal experiment using an arbitrary waveform generator, where a maximum error of 8 ns can be observed. Further studies were also carried out to quantify the effect of the influential factors on the group delay measurement. The results showed that altering the aperture has negligible effect of less than 50 ps on the group delay measurements. However, using too small of an aperture setting, which we assume to be lower than 0.05 MHz, may cause potential increase in measurement jitter and further contribute to the uncertainty budget.

Then, validation experiments with preferred parameter settings derived from the preceding discussion on different instruments representing the three methods were carried out on a typical antenna cable as well as four ordinary coaxial cables. Finally, the results showed hundred-picosecond consistency. However, we noted that although agreed within the evaluated uncertainty range, the measurement on the 50 m antenna cable under time interval method tended to show an overestimation of about 600 ps. Thus, given the widespread use of time interval measurement, the aforementioned measurements were compared to find the intersections of the TIC method and the reference simulator method, where the results are in alignment within their uncertainty ranges. The results showed that, faster external time pulses with lower counter trigger level are more recommended for time interval measurements on coaxial cables with high attenuation such as the GNSS antenna cables, that is, to be specific, less than 1.1 V when the pulse rise time is in the range of (2.5–5.5) ns and lower by varying degrees as the rise time decreases.

Data availability statement

The data cannot be made publicly available upon publication because they are not available in a format that is sufficiently accessible or reusable by other researchers. The data that support the findings of this study are available upon reasonable request from the authors.

Acknowledgments

This work was supported by the National Key R&D Program of China with Grant No. 2021YFB3900704, the National Natural Science Foundation of China with Grant No. 12473072 and the Open Foundation of National Railway Intelligence Transportation System Engineering Technology Research Center (2023YJ360).

ORCID iDs

Tian Yu https://orcid.org/0009-0001-1107-5492
Kun Liang https://orcid.org/0000-0002-1150-973X

References

[1] Petit G and Defraigne P 2023 Calibration of GNSS stations for UTC *Metrologia* **60** 025009
[2] Siccardi M, Rovera D and Romisch S 2016 Delay measurements of PPS signals in timing systems *2016 IEEE Int. Frequency Control Symp. (IFCS)* (IEEE) pp 1–6
[3] Hamza G G 2020 Timing pulses through coaxial cables *IEEE Instrum. Meas. Mag.* **23** 46–51
[4] Niessner A and Mache W *EUROMET Report* (available at: www.euramet.org/Media/docs/projects/828_TIME_Final.pdf)
[5] Valat D and Delporte J 2020 Absolute calibration of timing receiver chains at the nanosecond uncertainty level for GNSS time scales monitoring *Metrologia* **57** 025019
[6] Garbin E, Defraigne P, Krystek P, Piriz R, Bertrand B and Waller P 2019 Absolute calibration of GNSS timing stations and its applicability to real signals *Metrologia* **56** 015010
[7] Yu T, Liang K and Wei B 2023 Study on measurement methods for GNSS antenna cable delay *2023 Joint Conf. of the European Frequency and Time Forum and IEEE Int. Frequency Control Symp. (EFTF/IFCS)* pp 1–4
[8] Rovera D, Abgrall M, Uhrich P and Siccardi M 2015 Techniques of antenna cable delay measurement for GPS time transfer *2015 Joint Conf. IEEE Int. Frequency Control Symp. & the European Frequency and Time Forum* (IEEE) pp 239–44
[9] Petit G, Lewandowski W, Jiang Z, Arias F and Tisseran L BIPM guidelines for calibration (available at: ftp://ftp2.bipm.org/pub/tai/publication/gnss-calibration/guidelines/)
[10] Porat D I 1973 Review of sub-nanosecond time-interval measurements *IEEE Trans. Nucl. Sci.* **20** 36–51
[11] Kalisz J 2004 Review of methods for time interval measurements with picosecond resolution *Metrologia* **41** 17–32
[12] Hamza G G 2014 Investigation of the optimum trigger level in time interval measurement *Mapan* **29** 255–60
[13] Collin R E 2007 *Foundations for Microwave Engineering* (*Wiley*)
[14] Ostwald O *Rhode & Schwarz Application Note* (available at: https://cdn.rohde-schwarz.com.cn/pws/dl_downloads/dl_application/application_notes/1ez35/1ez35_1e.pdf)
[15] SRS Inc. Stanford research systems SR620 user manual (available at: www.thinksrs.com/downloads/pdfs/manuals/SR620m.pdf)
[16] Krystek P, Manfredini E G and Piriz R *BIPM Report* (available at: https://webtai.bipm.org/ftp/pub/tai/publication/gnss-calibration/absolute/AKAL-GMV-FRe-1.1.pdf)
[17] Liang K, Feldmann T, Bauch A, Piester D, Zhang A and Gao X 2010 Performance evaluation of NIM GPS receivers in use for time transfer with PTB *EFTF-2010 24th European Frequency and Time Forum* (IEEE) pp 1–8